J Neuropathol Exp Neurol

Vol. 73, No. 7
July 2014
pp. 658–670

ORIGINAL ARTICLE

Defining Peripheral Nervous System Dysfunction in the SOD-1^{G93A} Transgenic Rat Model of Amyotrophic Lateral Sclerosis

Nilo Riva, MD, PhD, Linda Chaabane, PhD, Marco Peviani, PhD, Daniela Ungaro, MD, Teuta Domi, PhD, Giorgia Dina, BS, Francesca Bianchi, MD, Giorgia Spano, BS, Federica Cerri, MD, Paola Podini, BS, Massimo Corbo, MD, Ubaldo Del Carro, MD, Giancarlo Comi, MD, Caterina Bendotti, PhD, and Angelo Quattrini, MD

Abstract

Growing evidence indicates that alterations within the peripheral nervous system (PNS) are involved at an early stage in the amyotrophic lateral sclerosis (ALS) pathogenetic cascade. In this study, magnetic resonance imaging (MRI), neurophysiologic analyses, and histologic analyses were used to monitor the extent of PNS damage in the hSOD-1^{G93A} ALS rat model. The imaging signature of the disease was defined using in vivo MRI of the sciatic nerve. Initial abnormalities were detected in the nerves by an increase in T_2 relaxation time before the onset of clinical disease; diffusion MRI showed a progressive increase in mean and radial diffusivity and reduction of fractional anisotropy at advanced stages of disease. Histologic analysis demonstrated early impairment of the blood-nerve barrier followed by acute axonal degeneration associated with endoneurial edema and macrophage response in motor nerve compartments. Progressive axonal degeneration and motor nerve fiber loss correlated with MRI and neurophysiologic changes. These functional and morphologic investigations of the PNS might be applied in following disease progression in preclinical therapeutic studies. This study establishes the PNS signature in this rat ALS model (shedding new light into pathogenesis) and provides a rationale for translating into future systematic MRI studies of PNS involvement in patients with ALS.

Key Words: Animal models, Magnetic resonance imaging, Motor nerve, Motor neuron disease, Neuropathy, Peripheral nerve.

From the Neuropathology Unit, Institute of Experimental Neurology (NR, LC, TD, GD, FC, GC, AQ) and Division of Neuroscience (NR, LC, DU, FB, FC, PP, UDC, GC, AQ), IRCCS San Raffaele Scientific Institute; Laboratory of Molecular Neurobiology, Department of Neuroscience, IRCCS Istituto di Ricerche Farmacologiche Mario Negri (MP, GS, CB); Department of Neurorehabilitation Sciences, Casa Cura Policlinico (MC); and Vita e Salute San Raffaele University (GC), Milan, Italy.

Send correspondence and reprint requests to: Nilo Riva, MD, PhD, Institute of Experimental Neurology and Department of Neurology, San Raffaele Scientific Institute, via Olgettina 48, Milan 20132, Italy; E-mail: riva.nilo@hsr.it.

This work was supported by Merck Serono SA (Geneva, Switzerland), a biopharmaceutical division of Merck KGaA (Darmstadt, Germany). Caterina Bendotti received funding from the European Community's Seventh Framework Program (FP7/2007-2013) under grant agreement EUROMOTOR (Grant No. 259867).

Supplemental digital content is available for this article. Direct URL citations appear in the printed text and are provided in the HTML and PDF versions of this article on the journal's Web site (www.jneuropath.com).

INTRODUCTION

Amyotrophic lateral sclerosis (ALS) is the most common and most severe form of motor neuron disease, leading to death 2 to 5 years after diagnosis (1, 2). The etiology and pathogenesis of human ALS remain unknown, and pharmacologic intervention has been ineffective to date (3).

Motor neurons are extremely polarized cells; the length of axons represents 90% of the total cell volume and exceeds the dimension of the neuronal cell body by several orders of magnitude. Axons are fundamental to anterograde and retrograde axonal transport, which are essential for neuronal differentiation, survival, and function. Peripheral axons may be involved in the pathogenetic cascade in ALS, and axonal loss is considered to be a major cause of signs and symptoms in human neurodegenerative disorders (4).

Although most studies on animal models are performed on the spinal cord, evidence derived from studies in transgenic mice overexpressing the mutated form of human superoxide dismutase 1 (hSOD-1^{G93A}) indicates that the first event in the disease process is the destruction of neuromuscular junctions, which occurs before motoneuron degeneration in the ventral horns of the spinal cord and before onset of clinical signs (5–7). Despite this, axonal damage within the peripheral nervous system (PNS) has not been extensively examined in humans or in animal models of ALS (8).

The ALS rat model expressing the mutated form of hSOD-1^{G93A} exhibits features that closely recapitulate the clinical and histopathologic features of the human disease (9). Furthermore, the larger size of rats is advantageous for in vivo analyses and provides greater availability of PNS and CNS tissues for pathologic studies (10). Our aim was to characterize in detail the natural history of PNS damage in the hSOD-1^{G93A} ALS rat model using both in vivo and ex vivo analyses. We provide an exhaustive functional and pathologic description of PNS involvement in the hSOD-1^{G93A} ALS rat model that could be applied to quantitative analysis in preclinical research studies on ALS.

MATERIALS AND METHODS

Experimental Design

Experiments were performed on genetically modified female Sprague-Dawley rats expressing a mutated (G93A)

human *SOD-1* gene (hSOD-1^{G93A} ALS rats; Taconic Farms, Germantown, NY) and wild-type (WT) nontransgenic littermates. Rats were bred and housed in specific pathogen free animal facilities on standard laboratory feed. Based on each animal's age and behavioral studies, hSOD-1^{G93A} ALS rats were divided into 5 groups according to disease stage and corresponding to the following time points: 60 to 70 days, normal stage; 80 to 90 days, presymptomatic stage; 95 to 110 days, subclinical stage (initiation of body weight loss); 115 to 125 days, muscle weakness stage (disease onset: 4/5 hindlimbs, 1/5 forelimbs); more than 130 days, end-stage disease (disease onset: 3/4 hindlimbs, 1/4 forelimbs) (10). Procedures involving animals and their care were conducted according to Mario Negri institutional guidelines, which are in compliance with national (DL no. 116, GU suppl. 40, February 18, 1992, circular no. 8, GU, 14 luglio 1994) and international laws and policies (EEC Council Directive 86/609, OJ L 358, 1, December 12, 1987; NIH Guide for the Care and Use of Laboratory Animals, US National Research Council, 1996).

To evaluate the degree of damage in the PNS, we performed in vivo functional tests through all time points (n = 4–6 rats per time point) with magnetic resonance imaging (MRI) of the sciatic nerves and electrophysiologic measurements, including assessment of motor action potentials and electromyography (EMG). After in vivo studies, subgroups of transgenic rats (n = 2–5 rats per time point) were killed for morphologic analysis. For each time point, 2 to 3 WT rats underwent MRI, neurophysiologic analyses, and morphologic analyses as controls.

Magnetic Resonance Imaging

All MRI experiments were conducted on a 3-T MRI scanner (Biospec; Bruker Biospin, Billerica, MA), with animals maintained under anesthesia using 1.5% to 2.0% isoflurane mixed with oxygen and under constant respiratory control. Serial MRI examinations were performed along the sciatic nerves (left and right sides) from hip level to knee level with acquisition of transversal relaxivity time (T_2) maps using a multiecho sequence with 8 echoes (echo time = 10–80 milliseconds), a repetition time of 4,000 milliseconds, and a spatial resolution of 156 × 287 μm^2 with 15 to 18 slices of 1.4 mm thickness. Diffusion tensor imaging data were acquired from coronal sections with a diffusion-weighted echo planar imaging sequence with a *b* value of 1,000 seconds/mm^2 applied in 6 directions with 2 reference images without a diffusion gradient and using the following parameters: repetition time of 3,000 milliseconds, echo time of 31.7 milliseconds, spatial resolution of 219 × 275 μm^2, and slice thickness of 1.4 mm. From these series of diffusion-weighted images, directional diffusivities of water molecules in white matter were separated into 2 components: axial diffusivity describing water diffusion along fibers ($\lambda_{||}$) and radial diffusivity describing water diffusion across fibers ($\lambda_{\perp}$). Maps of these components were calculated using the Bruker program (Paravision 5.1) to extract fractional anisotropy (FA), mean diffusivity (MD), and eigenvalues of the tensor ($\lambda_1, \lambda_2, \lambda_3$). Axial diffusivity ($\lambda_{||}$) and radial diffusivity ($\lambda_{\perp}$) were calculated as $\lambda_{||} = \lambda_1$; $\lambda_{\perp} = (\lambda_2 + \lambda_3) / 2$. Regions of interest within the sciatic nerve were defined manually in consecutive sections of both T_2 maps (almost 17 slices) and diffusion tensor imaging maps (3–4 slices).

Electrophysiologic Measurements

Electroneurography was performed following a previously described protocol in mice (11). Briefly, sciatic motor nerve conduction velocity (NCV) was obtained by stimulating the nerve with steel monopolar needle electrodes. To obtain 3 distinct sites of stimulation along the nerve, we inserted a pair of stimulating electrodes near the nerve at the ankle at the ischiatic notch and in paraspinal muscles, with the recording electrode placed at the point of intersection of the 2 perpendicular lines passing close to the spinal processes and the iliac crest to stimulate L4 to L6 roots. Compound motor action potential (cMAP) was recorded as described using a pair of recording needle electrodes; the active electrode was inserted in the muscles in the middle of the paw, and the reference electrode was placed in the skin between the first digit and the second digit (11). Nerve conduction velocity was measured by dividing the distance between the 2 points of stimulation by the difference in proximal and distal cMAP latencies, and cMAP amplitude was measured from peak to peak. Nerve conduction velocity and cMAP amplitudes were similarly recorded at the forelimbs: A pair of stimulating electrodes was inserted, respectively, near the nerve at the wrist and at paraspinal level C7, and cMAP was recorded from paw muscles.

Electromyography analysis was performed according to a standard protocol (11). Concentric bipolar needle EMG electrodes were used (size 25 mm × 30 G; Teca Elite; CareFusion, Middleton, WI). Spontaneous/involuntary EMG activities suggestive of denervation (including fibrillations, positive sharp waves, fasciculations, and complex repetitive discharges) were recorded. For each animal, the following bilateral muscles were analyzed: gastrocnemius, quadriceps, biceps, and triceps brachii.

Morphologic Studies

To perform comparative studies with in vivo analysis, we investigated the pathologic aspects of the sciatic nerves at different time points in hSOD-1^{G93A} ALS and control rats. To determine the involvement and progression of damage through the PNS, we also investigated some other peripheral nerves, including spinal motor and sensory roots, phrenic nerves, and nerves of the forelimbs (lateral and medial anterior thoracic, musculocutaneous, median, radial, and ulnar nerves) and hindlimbs (quadriceps and saphenous nerves). Bilateral nerves were harvested. Tissues were removed and fixed with 2% glutaraldehyde in 0.12 mol/L phosphate buffer, postfixed with 1% osmium tetroxide, and embedded in Epon (Fluka). Semithin sections (0.5–1 μm thick) were stained with toluidine blue and examined by light microscopy (Olympus BX51). Ultrathin sections (100–120 nm thick) were stained with uranyl acetate and lead citrate and examined by electron microscopy (Leo 912 Omega) (12).

Morphometric Analysis

Digitized nonoverlapping semithin section images from corresponding levels of the sciatic nerve were obtained with a digital camera (Leica DFC300F) using a 100× objective. For

each nerve, at least 5 nonoverlapping images were acquired. The numbers of myelinated and degenerating nerve fibers and transverse sectional areas were quantified using ImageJ software (National Institutes of Health, Bethesda, MD), and densities were then calculated (13).

Statistical Analysis

All results are presented as mean ± SD. Magnetic resonance imaging (T_2, MD, FA, $\lambda_{||}$, and $\lambda_{\perp}$ values), electrophysiologic, and morphometric data differences were assessed using 2-way analysis of variance (ANOVA) to compare time point (1–5) and group (hSOD-1^{G93A} ALS vs WT rats). Post hoc multiple comparisons were evaluated using the Bonferroni test after ANOVA. Correlations between morphometric analysis, distal cMAP amplitude, and mean T_2, MD, FA, $\lambda_{||}$, and $\lambda_{\perp}$ values of each sciatic nerve were investigated with Spearman rank correlation ρ. Statistical significance was considered at $p < 0.05$. All statistical tests were performed using SPSS software (SPSS Inc, Chicago, IL).

RESULTS

Magnetic Resonance Imaging

The progression of sciatic nerve damage was assessed according to specific criteria. Starting from the subclinical stage, the sciatic nerves of hSOD-1^{G93A} ALS rats appeared enlarged and hyperintense on T_2-weighted images versus those of age-matched control rats (Figs. 1A–E, 2A–C). These features were measured on axial sections of the nerves and were associated with an increase in transverse T_2 relaxation time in hSOD-1^{G93A} ALS rats. Two-way ANOVA of T_2 maps yielded a significant interaction between time point and group ($F_{4,1583} = 34.856$, $p < 0.001$) (Fig. 2D). Post hoc analysis showed a significant increase in mean T_2 values in hSOD-1^{G93A} ALS rats versus controls starting from the presymptomatic stage ($p < 0.001$). These data provide in vivo evidence of early damage in the sciatic nerves.

Progressive nerve damage was further confirmed by MRI diffusion techniques with a significant increase in diffusivity within the sciatic nerves (both MD and $\lambda_{\perp}$) starting from a more advanced stage of disease (Figs. 2E–G). Two-way ANOVA of MD, $\lambda_{\perp}$, and FA values yielded a significant interaction between time point and group ($F_{4,477} = 4{,}181$, $p < 0.005$; $F_{4,472} = 4{,}204$, $p < 0.005$; and $F_{4,477} = 2{,}627$, $p < 0.05$, respectively). Post hoc analysis showed a significant increase in MD and $\lambda_{\perp}$ values and a significant decrease in FA values in hSOD-1^{G93A} ALS rats versus controls starting from the subclinical stage ($p < 0.05$; muscle weakness stage, $p < 0.005$; end stage, $p < 0.0001$), muscle weakness stage ($p < 0.005$; end stage, $p < 0.001$), and end stage ($p < 0.005$), respectively. No significant interaction for axial diffusivity ($\lambda_{||}$) values was found.

Electrophysiologic Measurements

Neurophysiologic examination of 4 limbs allowed for a noninvasive and quantitative analysis of PNS motor fiber damage during disease progression (Figs. 3A–F); complete results are reported in Table, Supplemental Digital Content 1, http://links.lww.com/NEN/A595. Two-way ANOVA of distal cMAP amplitude values yielded a significant interaction between time point and group for both forelimbs ($F_{4,62} = 3.469$, $p < 0.05$) (Figs. 3A–C) and hindlimbs ($F_{4,62} = 5.394$, $p < 0.001$) (Figs. 3D–F). Post hoc comparisons revealed a significant reduction of distal cMAP amplitude in hSOD-1^{G93A} ALS rats that started in the muscle weakness stage and was more pronounced at end-stage disease ($p < 0.05$ and $p < 0.005$, respectively; Table, Supplemental Digital Content 1, http://links.lww.com/NEN/A595). A parallel significant reduction of cMAP amplitudes obtained from proximal stimulation (hindlimbs: ischiatic notch and paraspinal levels L4–L6; forelimbs: paraspinal level C7) was also observed. No significant differences in distal latency or NCV were observed, although a tendency toward a reduction of NCVs was noted in the most advanced stages of disease. Needle examination showed abundant signs of acute active denervation starting from the muscle weakness stage (Table, Supplemental Digital Content 2, http://links.lww.com/NEN/A596). In most hSOD-1^{G93A} ALS rats, signs of acute denervation appeared abruptly; in only a few cases were they preceded by signs of spontaneous activity (such as fasciculations, increased peri-insertional activity, or complex repetitive discharges) at the presymptomatic and subclinical stages (Figs. 3G–M).

Morphologic Studies

To validate the in vivo findings, we first compared the MRI data of the sciatic nerve with histopathologic analysis. At the preclinical stage, semithin section analysis showed a normal distribution of nerve fibers (similar to that of WT control nerves) without any signs of axonal damage (Figs. 1A, B). Starting from the subclinical stage, a few ovoids, indicating acute axonal degeneration, were present in the endoneurium (Fig. 1C). In advanced stages of disease, there were patchy lesions characterized by axonal degeneration, macrophages infiltrating the endoneurium, reduction of myelinated nerve fibers, and endoneurial edema (Figs. 1D, E). Clusters of small myelinated fibers, indicating axonal regeneration, were not observed.

Electron microscopy examination showed endoneurial blood vessel abnormalities starting from the preclinical stage (i.e. several days before the appearance of signs of axonal degeneration in semithin sections). In particular, we observed distension of tight junction gaps; in some instances, the junctions appeared to be open between endothelial cells, which displayed cytoplasmic expansion and increased numbers of mitochondria, vesicles, and abnormal basement membranes (Figs. 1F–H). Proteinaceous fluid was noted in the vicinity of blood vessels. These data, along with the presence of endoneurial edema adjacent to capillaries, suggest an altered blood-nerve barrier in hSOD-1^{G93A} ALS rats and may represent the pathologic basis for the increase in T_2 relaxation time values observed in vivo by MRI at the early stages of disease.

Morphometric analysis confirmed an increase in the number of degenerating fibers starting from the presymptomatic stage. Two-way ANOVA of myelinated fiber density yielded a significant interaction between time point and group ($F_{4,334} = 7.486$, $p < 0.001$); post hoc analysis showed a significant decrease in hSOD-1^{G93A} rat sciatic nerve fiber density starting from the subclinical stage versus controls ($p < 0.0001$)

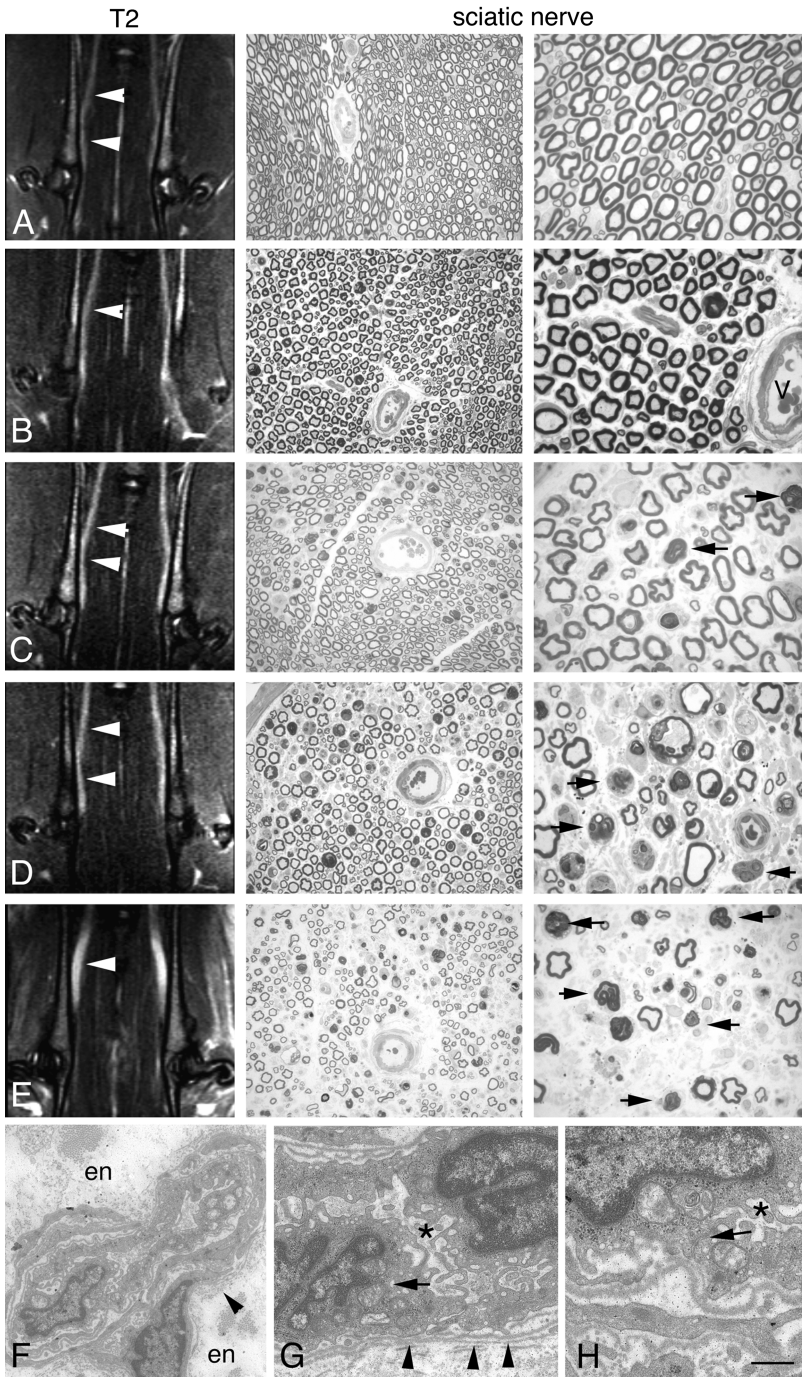

FIGURE 1. Conventional MRI (T_2-weighted images; left) and morphologic (sciatic nerve) analyses of WT and hSOD-1^{G93A} ALS rats at different time points. **(A)** Wild-type sciatic nerves were slightly hyperintense (arrowheads) versus muscle tissue; transverse semithin sections showed the normal appearance of sciatic nerve. Scale bars = **(center)** 40 μm; **(right)** 20 μm. **(B)** At the presymptomatic stage, T_2 signals were similar to baseline examination (arrowhead); semithin sections showed slight perivascular endoneurial edema (V, vessel). **(C–E)** Starting from the subclinical stage (95–110 days), the sciatic nerves appeared enlarged and hyperintense on T_2-weighted images (**C**, arrowheads). There was a progressive increase in T_2 signal during the course of the disease (**D**; 116 days, muscle weakness stage) and at 130 days (**E**; end-stage disease) (arrowheads). Transverse semithin sections showed few signs of axonal degeneration starting from the subclinical stage (**C**, arrows). Many ovoids (indicating acute axonal degeneration) and marked fiber loss were noted in advanced stages of disease (**D, E**, arrows). **(F–H)** Electron microscopy showed endoneurial vessels in the sciatic nerve at the preclinical stage (80–90 days). Note proteinaceous edema in the endoneurium (en) in **(F)** and fragmented endothelial basal lamina (arrowheads) **(F, G)**. Asterisks in **(G)** and **(H)** indicate open tight junctions between endothelial cells showing an increase in the numbers of cytoplasmic vesicles and abnormal mitochondria (arrows in **G, H**). Scale bars = (**A–E**, middle) 40 μm; (**A–E**, right) 20 μm; **(F)** 2 μm; **(G, H)** 1 μm.

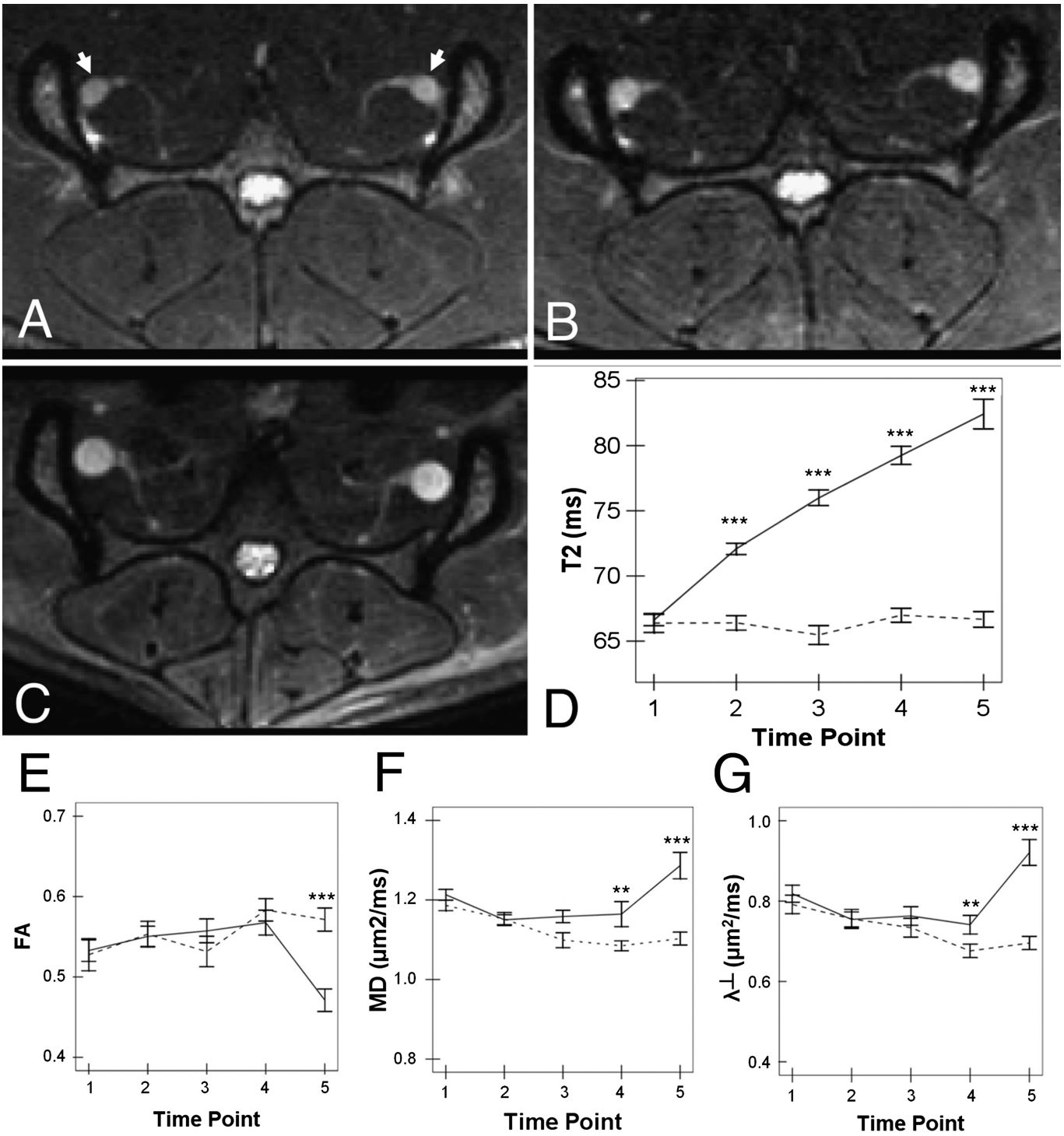

FIGURE 2. (A–C) Examples of T_2-weighted axial images along the sciatic nerve (arrows), acquired from hSOD-1^{G93A} ALS rats at the presymptomatic stage (90 days; **A**), subclinical stage (123 days; **B**), and end stage (>130 days; **C**), showing progressive hypertrophy and signal increase in the nerves. **(D)** Quantification of transverse (T_2) relaxation time further highlighted disease progression with a significant T_2 increase, starting from the presymptomatic stage. **(E–G)** Fractional anisotropy was significantly decreased at end-stage disease **(E)**, whereas MD **(F)** and, in particular, radial diffusivity ($\lambda_\perp$; **G**) were increased, starting from the muscle weakness stage. Continuous line: hSOD-1^{G93A} ALS rats; dotted line: WT. ** $p < 0.005$, *** $p < 0.0005$ versus WT on 2-way ANOVA and Bonferroni post hoc test. Values are presented as mean ± SE.

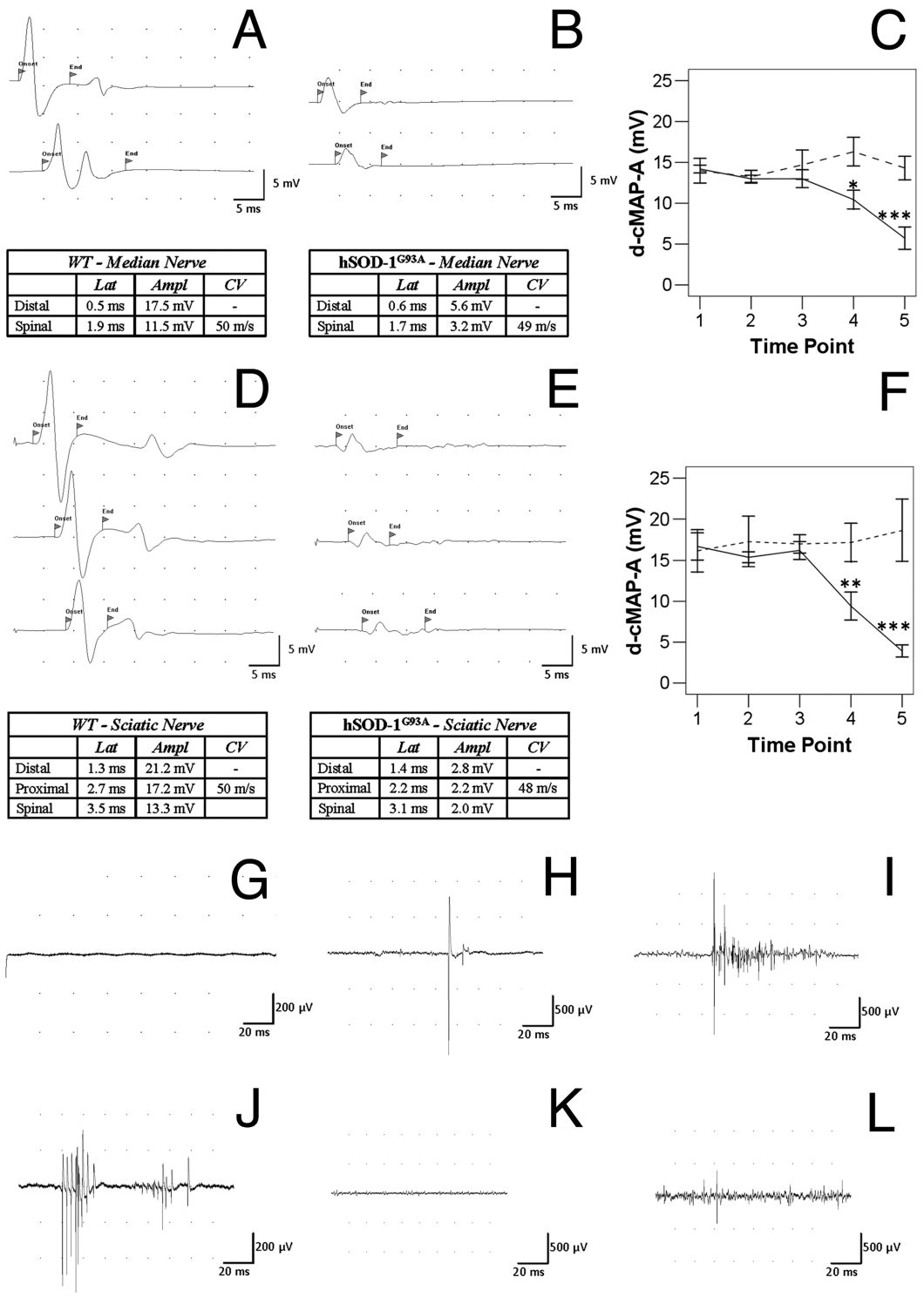

WT - Median Nerve			
	Lat	Ampl	CV
Distal	0.5 ms	17.5 mV	-
Spinal	1.9 ms	11.5 mV	50 m/s

hSOD-1^{G93A} - Median Nerve			
	Lat	Ampl	CV
Distal	0.6 ms	5.6 mV	-
Spinal	1.7 ms	3.2 mV	49 m/s

WT - Sciatic Nerve			
	Lat	Ampl	CV
Distal	1.3 ms	21.2 mV	-
Proximal	2.7 ms	17.2 mV	50 m/s
Spinal	3.5 ms	13.3 mV	

hSOD-1^{G93A} - Sciatic Nerve			
	Lat	Ampl	CV
Distal	1.4 ms	2.8 mV	-
Proximal	2.2 ms	2.2 mV	48 m/s
Spinal	3.1 ms	2.0 mV	

FIGURE 3. Neurophysiologic findings in WT and hSOD-1^{G93A} ALS rats. **(A, B, D, E)** Representative ENG findings. Recordings of median nerve **(A, B)** and sciatic nerve **(D, E)** cMAP in WT **(A, D)** and hSOD-1^{G93A} ALS rats **(B, E)** at end-stage disease. Note the marked decline in cMAP amplitude in hSOD-1^{G93A} ALS rats. **(C–F)** On 2-way ANOVA, there was a statistically significant decline in mean distal cMAP amplitude (d-cMAP) starting from muscle weakness stage at both forelimbs **(C)** and hindlimbs **(F)** (continuous line: hSOD-1^{G93A} ALS; dotted line: WT). * $p < 0.05$, ** $p < 0.005$, *** $p < 0.0005$ versus WT. Values are presented as mean ± SE. Representative EMG findings in hSOD-1^{G93A} ALS rats. At early stages, the muscle was electrically silent **(G)**; at the presymptomatic and subclinical stages in some cases, fasciculations **(H)**, increased peri-insertional activity **(I)**, complex repetitive discharges **(J)**, or initial denervation activity (**K**, positive sharp waves and fibrillation potentials) was recorded; however, in most cases, an abrupt appearance of abundant signs of acute active denervation was observed **(L)**, starting from the muscle weakness stage.

(Fig. 4A). Two-way ANOVA of degenerating fiber density yielded a significant interaction between time point and group ($F_{4,1883} = 8.844$, $p < 0.001$); post hoc analysis showed a significant increase in hSOD-1^{G93A} rat sciatic nerves starting from the presymptomatic stage ($p < 0.001$) (Fig. 4B). Hence, reduction of fiber density at the subclinical stage was not accompanied by a significant increase in the number of degenerating axons and could therefore be explained by an increase in interstitial space secondary to endoneurial edema, as highlighted by semithin sections and electron microscopy.

The histopathologic characteristics of the PNS of hSOD-1^{G93A} ALS rats were consistent with acute motor axonal neuropathy/neuronopathy. At the muscle weakness stage, the coexistence of variable percentages of pathologic and normal nerves was observed within the same animal. In both hindlimbs and forelimbs, semithin sections showed classical acute axonal degeneration, reduction of myelinated nerve fibers, and endoneurial edema, which followed the topographic distribution of motor fibers in mixed nerves (Figs. 4C–I; Figure, Supplemental Digital Content 3, http://links.lww.com/NEN/A597). In all animals killed at different time points, the saphenous nerve (which is pure sensory) was spared and found to be normal at all disease stages (data not shown); this was also true for dorsal roots. From the subclinical stage to the end stage, lesions of motor nerve roots were found in all hSOD-1^{G93A} ALS rats (Figure, Supplemental Digital Content 4, http://links.lww.com/NEN/A598).

Peripheral nervous system damage varied in degree and nerve distribution among animals killed at the same time point. In the hindlimbs, semiquantitative grading of nerve pathologic abnormalities showed a consistently similar amount of axonal damage within the quadriceps nerves on both sides within the same animal (spinal segments L2–L4; Figs. 5A, B) and within the sciatic nerves on either side (spinal segments L4–L6; Figs. 5C, D). Similarly, in the forelimbs, a similar amount of nerve damage was observed not only when comparing the same nerve of either side but also when comparing different nerves within the same limb; more precisely, a similar amount of axonal damage was observed both between the lateral anterior thoracic and musculocutaneous nerves (both originating from spinal segments C6–C7; Figs. 5E–H) and between the medial anterior thoracic and ulnar nerves (both originating from spinal segments C8–T1; Figs. 5I–M) (16).

Axonal degeneration was invariably accompanied by inflammatory infiltrates (mainly activated foamy macrophages) and endoneurial edema (Fig. 6). In the perineurium, some eosinophil granulocytes and lymphocytes (mainly in the perivascular space) were occasionally observed in few nerves (Figs. 6A–C). Immunocytochemistry showed macrophage inflammatory infiltrates (CD11-positive), which were predominantly in close contact with axons in the sciatic nerves (Figs. 6D, E). Some cells were positive for the T-cell marker CD3 (Fig. 6F).

Correlation Analysis

Results of correlation analysis are summarized in the Table and graphed in Figure, Supplemental Digital Content 5, http://links.lww.com/NEN/A599. Reduction of nerve fibers in the sciatic nerves corresponded to higher T_2 values, which are related to an increase in relative water content within tissues. Fiber density reduction also corresponded to an increase in MD and $\lambda_\perp$ values, which represent the MD properties of water molecules in any direction and perpendicular to the longitudinal axis of the nerve, respectively. Instead, reduction of nerve fiber density was related to a decrease in FA values, a measure of the degree of the preferential diffusivity direction of water molecules. Significant correlations between the density of degenerating fibers and MRI parameters were also found; correspondingly, they displayed opposite algebraic signs of the Spearman correlation coefficient ρ. No significant correlations were found between morphometric data and $\lambda_\parallel$ values. Higher values of sciatic nerve myelinated fiber density were related to increasing values of cMAP amplitude, an electrophysiologic measure of axonal integrity. Correspondingly, axonal degeneration and loss of nerve fibers were related to reduced cMAP amplitude values. No significant correlations were found between morphometric data and distal latency or conduction velocity values.

DISCUSSION

The information conveyed by MRI and neurophysiologic studies was complementary, and both techniques allowed for a quantitative in vivo analysis of the natural history of the disease. Magnetic resonance imaging allowed for the detection and quantification of nerve alterations. High sensitivity to initial damage, starting from the presymptomatic stage, was demonstrated for T_2 relaxation time, a parameter influenced by tissue water content. At this early time point, histopathologic analysis in hSOD-1^{G93A} rats did not show evidence of axonal degeneration but highlighted an impairment of the blood-nerve barrier associated with an increase in water content.

We showed that there was ultrastructural evidence for early blood-nerve barrier abnormalities that occurred before the initiation of axonal damage and fiber loss. This observation is in agreement with previous studies showing blood-brain or blood–spinal cord barrier damage as one of the earliest pathologic events in the ALS toxic cascade, further supporting the notion of ALS as a noncell autonomous disease of motor neurons (14). The blood-nerve barrier dysfunction could result in the release of neurotoxic products and reductions in microcirculation and hypoperfusion, potentially contributing to the degeneration of large motor axons (15, 16). Subsequently, starting from the subclinical stage, the sciatic nerves appeared clearly enlarged and hyperintense on T_2-weighted images compared with age-matched control rats; this correlated with histopathologic evidence of progressive nerve damage, in particular axonal degeneration and fiber loss, associated with increased endoneurial edema. These findings are in agreement with and complementary to recent reports using MRI techniques, which showed that muscle degeneration in the experimental mouse model of ALS occurs before any evidence of neurodegeneration (17). Diffusion MRI, an imaging method that measures water directional diffusivities along fiber tracts, showed a significant increase in MD in hSOD-1^{G93A} rats at end-stage disease; this was in association with a reduction of FA, indicating a loss of the preferential diffusion direction along the nerve axolemma. Moreover, radial diffusivity ($\lambda_\perp$), which has been shown to increase during the degenerative phase after nerve crush injury (18), tended to increase

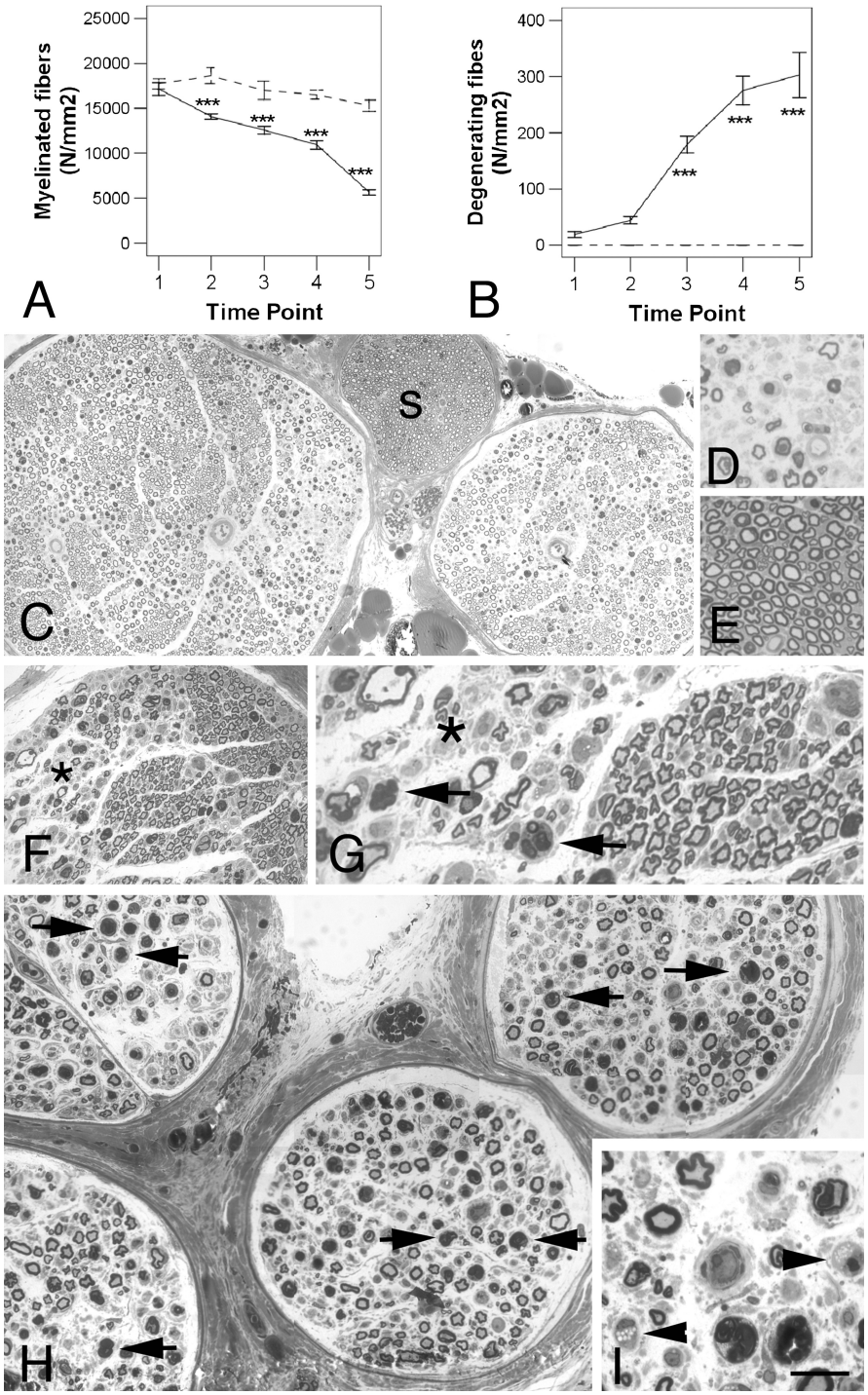

FIGURE 4. (A, B) Morphometric analysis of sciatic nerve fibers. On 2-way ANOVA, there was a statistically significant reduction of myelinating fibers starting from the presymptomatic stage **(A)** and a significant increase in degenerating fiber concentrations starting from the subclinical stage **(B)** (continuous line: hSOD-1^{G93A} ALS rats; dotted line: WT). *** $p < 0.0005$ versus WT on 2-way ANOVA and Bonferroni post hoc test. Values are presented as mean ± SE. **(C–I)** The hSOD-1^{G93A} ALS rats developed severe acute axonal neuropathy/neuronopathy in 4 limbs. Selective motor fiber damage in the sciatic (sensory-motor) nerve **(C–E)**: Reduction of nerve fibers and endoneurial edema followed the topographic distribution of motor fibers (**C**; S marks the sensory sural nerve); there was axonal degeneration in motor fibers **(D)** and normal nerve fibers in the sensory sural nerve **(E)**. **(F, G)** Transverse semithin sections of radial (sensory-motor) nerve **(F, G)**. Focal losses of myelinated fibers were preferentially located in the motor compartment (*) with active axonal degeneration (arrows); sensory fibers were spared. **(H, I)** Transverse semithin sections of quadriceps (motor) nerve. There was evidence of axonal degeneration (**H**, arrows) associated with endoneurial edema **(H)** and macrophage response (**I**, arrowheads). Scale bars = **(C, F)** 60 μm; **(D, E, H)** 40 μm; **(G)** 25 μm; **(I)** 10 μm.

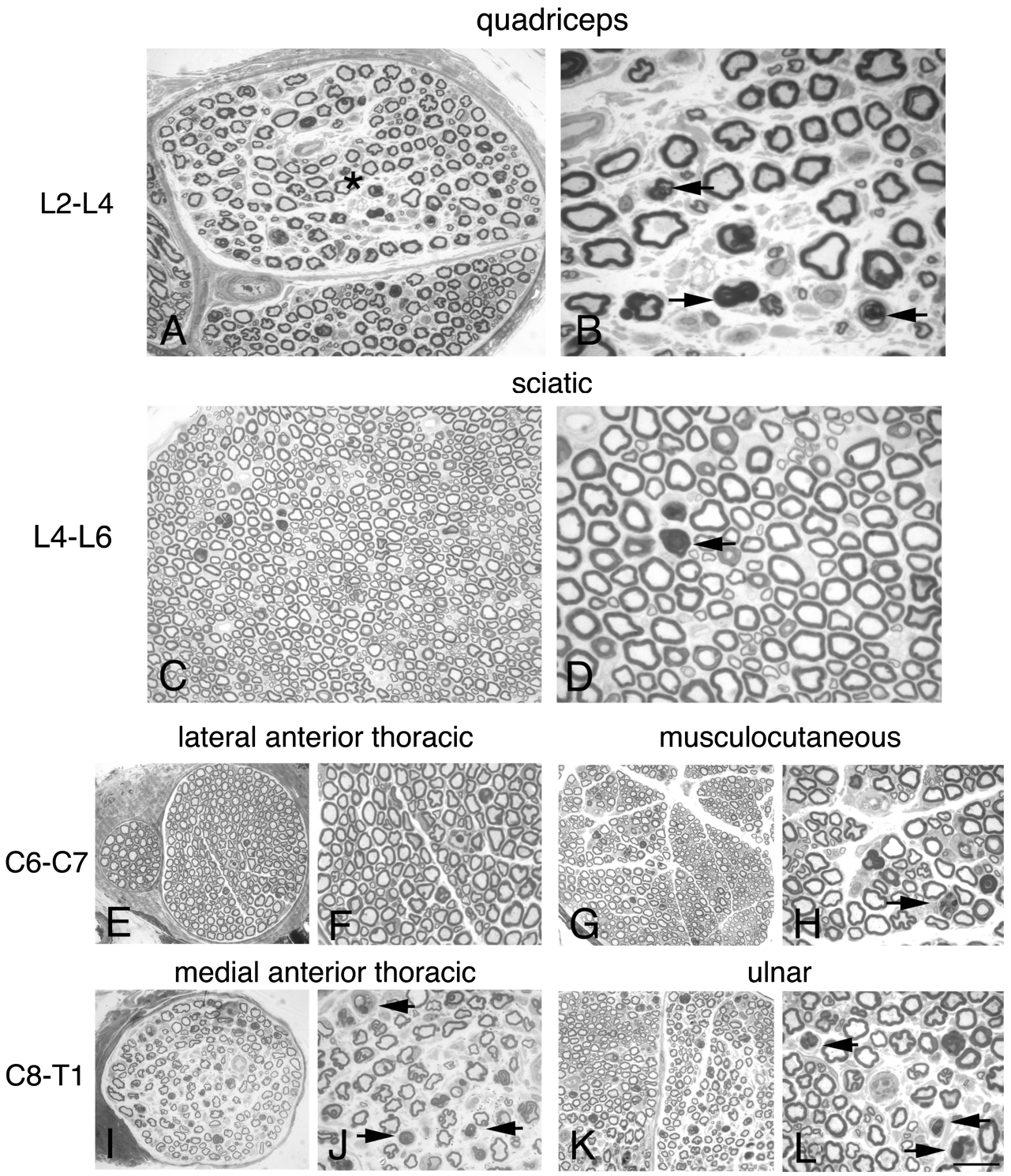

FIGURE 5. The hSOD-1^{G93A} ALS rats developed focal axonal damage. **(A–D)** Example illustrates the coexistence of pathologic and normal nerves at forelimbs and hindlimbs within the same animal. Transverse semithin sections of quadriceps nerves **(A)**, originating from spinal segments L2 to L4, showed mild focal reduction of motor nerve fibers (*), evidence of axonal degeneration (**B**, arrows), and endoneurial edema. Normal distribution and density of myelinated nerve fibers in the sciatic nerves **(C)**, originating from spinal segments L4 to L6, with minimal axonal damage (**D**, arrow). **(E–H)** Semithin sections of the lateral anterior thoracic **(E, F)** and musculocutaneous **(G, H)** nerves, both originating from spinal segments C6 to C7, showed normal density of myelinated nerve fibers **(F–H)** and few ovoids indicating axonal degeneration (**H**, arrow). **(I–L)** Semithin sections from the medial anterior thoracic **(I, J)** and ulnar **(K, L)** nerves, both originating from spinal segments C8 to T1, showed reduction of nerve fibers **(I, J)** and acute axonal degeneration (**L**, arrows). Scale bars = **(A, B, I, J, H, L)** 20 μm; **(B, D)** 10 μm; **(E, G, I, K)** 40 μm.

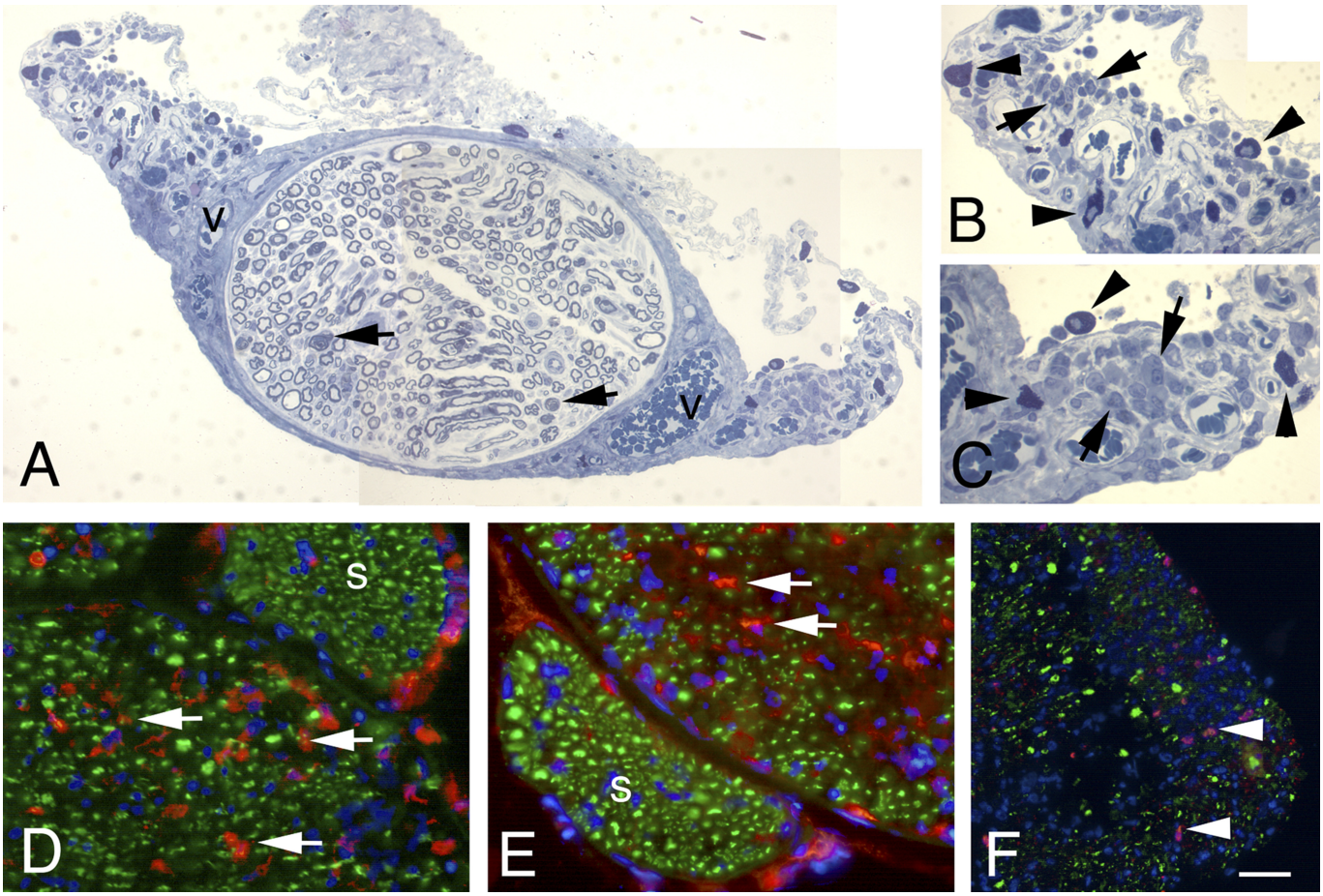

FIGURE 6. (A–C) Transverse semithin sections of phrenic nerve showed axonal degeneration (**A**, arrowheads) and inflammatory infiltrates in the epineurium: Lymphocytes (arrows; **B, C**) and mast cells (arrowheads; **B, C**) were located near epineurial vessels (v marks vessels; **A–C**). **(D–F)** Immunohistochemistry on transverse sciatic nerves from a 125-day-old hSOD-1^{G93A} ALS rat using anti-CD11 antibody (red in **D, E**) to identify macrophages; anti-neurofilament (green in **D–F**) to detect axons; and anti-CD3 (**F**, red) to identify T lymphocytes. Many macrophages were present in the endoneurium (arrows in **D, E**) but not in the sensory compartments (s marks the sural nerve in **D, E**). In anti-CD3–stained transverse sections, few T cells were identified (**F**, arrowhead). Scale bars = **(A, D–F)** 40 μm; **(B, C)** 15 μm.

starting from subclinical stage, reaching statistical significance at the muscle weakness stage, whereas diffusivity along fiber axes ($\lambda_{||}$) remained constant during the course of the disease.

Fiber density showed a significant correlation with all DTI measures, with the exception of $\lambda_{||}$ values. This might be explained by the fact that $\lambda_{||}$ is influenced by fiber integrity and alignment (which would lead to a positive correlation with fiber density) but also by water molecule diffusivity in the interstitial space; this, on the contrary, increases along with nerve fiber loss and endoneurial edema and, therefore, would lead to a counteracting negative correlation between $\lambda_{||}$ and fiber density. The strong correlation of MD and $\lambda_{\perp}$ with fiber density supports the idea that diffusivity reflects the increase in interstitial space, which is a consequence of endoneurial edema, as confirmed by histopathologic analysis. However, significant changes in MRI diffusivity properties were delayed compared with T_2 relaxation times, which might be explained by several factors. First, motor fibers in ALS are selectively compromised (as confirmed by our pathologic analysis), and the sciatic nerve is a mixed nerve composed of both motor and sensory nerve fibers that are not differentiated by MRI because of spatial resolution limitations. Thus, alterations in MRI diffusion parameters could be detectable when a critical number of fibers have undergone axonal degeneration. In addition, each myelinated nerve fiber in the PNS is surrounded by a basal lamina. After Wallerian degeneration of the axon, the basal lamina is preserved and forms an endoneurial tube that is essential for inducing axonal regeneration and the formation of bands of Büngner. Theoretically, endoneurial tubes might limit the anisotropic diffusion of water molecules, maintaining the high diffusivity of water molecules along fibers ($\lambda_{||}$).

Despite recent rapid progress, MRI techniques have, to date, been used almost exclusively in ALS patients for the study of the CNS. There have been only 2 single patient case reports describing gadolinium lumbar nerve root enhancement (19, 20) and 1 case report of cervical nerve root and brachial plexus enhancement in a probable case of ALS (21). The MRI findings highlighted here are in line with these reports and provide a rational basis for translating into future MRI studies

TABLE. Correlations Between Sciatic Nerve Morphometric, MRI, and Electroneurographic Parameters

Morphometry	Parameter	Spearman Correlation Coefficient *r*	p
MRI			
Normal fiber density	T_2 axial	−0.642	<0.001
	MD	−0.512	0.006
	FA	0.599	0.001
	$\lambda_{\perp}$	−0.566	0.002
	$\lambda_{\parallel}$	−0.093	NS
Degenerating fiber density	T_2	0.800	<0.001
	MD	0.150	NS
	FA	−0.500	0.008
	$\lambda_{\perp}$	0.421	0.029
	$\lambda_{\parallel}$	0.180	NS
Electroneurography			
Normal fiber density	d-cMAP-A	0.597	0.015
	p-cMAP-A	0.534	0.033
	CV	0.313	NS
Degenerating fiber density	d-cMAP-A	−0.673	0.004
	p-MAP-A	−0.567	0.022
	CV	0.283	NS

CV, conduction velocity; d-cMAP-A, distal cMAP amplitude; $\lambda_{\parallel}$, parallel diffusivity; $\lambda_{\perp}$, radial diffusivity; NS, not significant; p-cMAP-A, proximal cMAP amplitude; T_2, T_2-weighted axial value.

aimed at systematically assessing PNS involvement in ALS patients as an attempt to develop new potential biomarkers for clinical practice.

Complementary information was conveyed by the longitudinal in vivo neurophysiologic examination that showed an initial reduction of distal cMAP amplitude starting from 95 to 110 days and reaching statistic significance at 115 to 125 days. Correlation analysis confirmed a significant association between cMAP amplitude and the neuropathologic measure of sciatic nerve fiber density (22). Even though there are no detailed systematic neurophysiologic studies in SOD-1^{G93A} rats for comparison with the present study, a significant reduction of phrenic nerve cMAP amplitudes at 16 weeks of age (112 days) has been previously reported, consistent with our data (23). However, there are several reports concerning the use of these techniques in SOD-1^{G93A} mice, suggesting an earlier reduction of cMAP amplitude caused by the loss of neuromuscular connections before muscle weakness becomes evident (24–26). Interestingly, it has recently been shown in SOD-1 mice that, whereas cMAP amplitude displays a progressive linear decline in the tibialis anterior muscle, there is an immediate amplitude drop from 8 to 12 weeks of age in the plantar muscle (27). This trend of cMAP reduction is consistent with our data, suggesting an ongoing acute denervation process. This is also supported by the finding, starting from the subclinical stage, of acute denervation signs on needle examination (28). These data are consistent with the neurophysiologic findings reported in single case reports of ALS patients at the preclinical stage of disease (29, 30); however, although needle EMG recording of involuntary and spontaneous muscle activity is fundamental to early diagnosis in human patients (31), its usefulness decreases upon quantitative evaluation of disease progression. Therefore, this technique should be considered as a supporting tool for revealing the first signs of muscle denervation (24, 28). Further neurophysiologic studies using more sophisticated techniques may lead to a better understanding of the disease process, thus allowing for a better comparison of potential differences between the SOD-1^{G93A} rat model and the SOD-1^{G93A} mouse model.

Although much of the research on neurodegenerative disorders focuses on neuronal cell death and apoptosis pathways, recent evidence indicates that peripheral axons could be involved at an early stage in the ALS pathogenetic cascade (32–34), before the appearance of clinical disease and the loss of motor neurons (35, 36). In our study, morphologic analysis of different peripheral nerves also allowed us to gain insights into the kinetics and distribution of pathologic processes within the PNS of hSOD-1^{G93A} ALS rats. Nerve pathology develops focally at onset, subsequently spreading through the entire PNS. From the muscle weakness stage onward, we observed a sharp increase in the percentage of nerves displaying signs of axonal damage. Motor nerve fibers that were affected abruptly exhibited the characteristic features of acute axonal degeneration, including rapid appearance of axon fragmentation and removal of debris by activated macrophages, suggesting Wallerian degeneration or possible ''dying-back'' processes. Both of the abovepproposed mechanisms for distal axonal damage seem to occur in neurodegenerative diseases, including motor neuron disease.

Studies in hSOD-1^{G93A} transgenic mice indicate that the first event in this disease process is neuromuscular junction destruction, followed by ventral root axonal loss and, ultimately, motoneuron somata degeneration (5, 6, 37, 38). Neuromuscular junction degeneration may be partially compensated for, at least in the early stages of disease, by neuromuscular junction functional and morphologic changes such as distal nerve collateral sprouting (39–42); however, axonal degeneration remains a major determinant of disability in both rodent models and human

ALS patients (4). It cannot be compensated for by nerve regrowth, as supported by the absence of clusters of regenerating fibers in the present study and by previous reports in human ALS motor nerve biopsies (8). Considering that even a complete rescue of motor neuron cell bodies does not cure SOD-1 mutant mice (7, 41) and that recent advances in the field of axonal biology demonstrate that axons and neuronal cell body possess distinct pathways for survival and degeneration (6, 43–45), a better understanding of the pathogenetic events occurring within the PNS may hasten the development of new effective therapeutic approaches to ALS.

The damage in the PNS varied in degree and nerve distribution among animals analyzed at the same time point. The opportunity to harvest multiple nerves (from hindlimbs and forelimbs) allowed us to observe the coexistence of a variable percentage of pathologic and normal nerves within the same animal. A similar amount of nerve damage was observed not only in the same nerve on either side but also in different nerves within the same limb. Nerves originating from the same spinal segment/roots displayed a similar amount of damage, suggesting focal involvement of motor neurons at the onset. These data are consistent with focal onset of motor impairment, suggesting that the loss of lower motor neurons first occurs in a restricted region of the spinal cord and then propagates to other regions (46). We have shown that forelimb and hindlimb pathologies were similar, suggesting that, in therapeutic preclinical studies using the hSOD-1^{G93A} ALS rat model, stereologic analysis should include sampling of the whole spinal cord to ensure proper spatial mapping and quantification of the pathologic process. Alternatively, samples of multiple peripheral nerves originating from consecutive segments of the spinal cord could be considered.

Endothelial activation and subsequent endoneurial edema may well be the first morphologic detectable signs of a neuronflammatory process; indeed, we invariably observed neuroinflammation, mainly prominent macrophage infiltrates, in diseased nerves. Although involvement of neuroinflammation in both human ALS (47, 48) and animal models (49–51) has been reported, its role in pathogenesis is not clear (52–54). Recent work showed that macrophages may accumulate within the PNS and ventral horns of the spinal cord before the clinical onset of disease (55); however, although activated microglia may exhibit a protective role (M2) or a detrimental role (M1) in motor neurons in the CNS (56), the role of macrophages in peripheral nerves in ALS may be the phagocytic removal of debris after axonal degeneration (57, 58). Although the administration of anti-inflammatory or immunosuppressive drugs early in the disease has extended survival in the transgenic mouse model of ALS (59, 60), it has been clearly demonstrated that both innate immunity and adaptive immunity may have protective effects on disease progression in SOD-1 mutant mice (61). This suggests that a balance in immune response is essential for modulating the development and progression of the disease and might explain the lack of efficacy of immunosuppressive or immunomodulating drugs in human ALS patients to date (62–65). The hypothesis that some of the PNS-resident cells, such as endothelial or Schwann cells, could ''sense'' early axonal dysfunction or damage cannot be excluded (66, 67).

Defining PNS involvement in hSOD-1^{G93A} rats could be of value in following disease progression in preclinical therapeutic studies but could also provide clues for a ''PNS perspective'' into the disease pathogenetic process.

In summary, we have shown how the disease develops as acute motor axonal neuropathy/neuronopathy in the hSOD-1^{G93A} ALS rat model. It has been demonstrated that distal axonal damage and denervation may occur independently of motor neuron death in the spinal cord in SOD-1 mutant mice (35). Likewise, there are examples of treatments that show a significant antiapoptotic and neuroprotective effect on spinal motor neurons in vivo but fail to improve survival and/or motor performance in ALS rodent models. Therefore, a better understanding of the early steps in disease pathogenesis and progression could lead to new therapeutic strategies aimed at protecting the axon or interfering with mechanisms of denervation, thus preventing the spread of axonal degeneration to clinically unaffected body regions.

REFERENCES

1. Kiernan MC, Vucic S, Cheah BC, et al. Amyotrophic lateral sclerosis. Lancet 2011;377:942–55
2. Worms PM. The epidemiology of motor neuron diseases: A review of recent studies. J Neurol Sci 2001;191:3–9
3. Ludolph AC, Jesse S. Evidence-based drug treatment in amyotrophic lateral sclerosis and upcoming clinical trials. Ther Adv Neurol Disord 2009;2:319–26
4. Coleman MP, Perry VH. Axon pathology in neurological disease: A neglected therapeutic target. Trends Neurosci 2002;25:532–37
5. Fischer LR, Culver DG, Tennant P, et al. Amyotrophic lateral sclerosis is a distal axonopathy: Evidence in mice and man. Exp Neurol 2004;185:232–40
6. Fischer LR, Glass JD. Axonal degeneration in motor neuron disease. Neurodegener Dis 2007;4:431–42
7. Murray LM, Talbot K, Gillingwater TH. Review: Neuromuscular synaptic vulnerability in motor neurone disease: Amyotrophic lateral sclerosis and spinal muscular atrophy. Neuropathol Appl Neurobiol 2010;36:133–56
8. Riva N, Iannaccone S, Corbo M, et al. Motor nerve biopsy: Clinical usefulness and histopathological criteria. Ann Neurol 2011;69:197–201
9. Nagai M, Aoki M, Miyoshi I, et al. Rats expressing human cytosolic copper–zinc superoxide dismutase transgenes with amyotrophic lateral sclerosis: Associated mutations develop motor neuron disease. J Neurosci 2001;21:9246–54
10. Matsumoto A, Okada Y, Nakamichi M, et al. Disease progression of human SOD1 (G93A) transgenic ALS model rats. J Neurosci Res 2006;83:119–33
11. Bolino A, Bolis A, Previtali SC, et al. Disruption of Mtmr2 produces CMT4B1-like neuropathy with myelin outfolding and impaired spermatogenesis. J Cell Biol 2004;167:711–21
12. Riva N, Gallia F, Iannaccone S, et al. Chronic motor axonal neuropathy. J Peripher Nerv Syst 2011;16:341–46
13. Riva N, Domi T, Lopez ID, et al. The brachial plexus branches to the pectoral muscles in adult rats: Morphological aspects and morphometric normative data. Front Neuroanat 2012;6:41
14. Nicaise C, Mitrecic D, Demetter P, et al. Impaired blood-brain and blood-spinal cord barriers in mutant SOD1-linked ALS rat. Brain Res 2009;1301:152–62
15. Zhong Z, Deane R, Ali Z, et al. ALS-causing SOD1 mutants generate vascular changes prior to motor neuron degeneration. Nat Neurosci 2008;11:420–22
16. Garbuzova-Davis S, Rodrigues MC, Hernande-Ontiveros DG, et al. Amyotrophic lateral sclerosis: A neurovascular disease. Brain Res 2011;1398:113–25
17. Marcuzzo S, Zucca I, Mastropietro A, et al. Hind limb muscle atrophy precedes cerebral neuronal degeneration in G93A-SOD1 mouse model of amyotrophic lateral sclerosis: A longitudinal MRI study. Exp Neurol 2011;231:30–37

18. Morisaki S, Kawai Y, Umeda M, et al. In vivo assessment of peripheral nerve regeneration by diffusion tensor imaging. J Magn Reson Imaging 2011;33:535–42
19. Luigetti M, Cianfoni A, Conte A, et al. Gadolinium enhancement of the lumbar leptomeninges and roots in a case of ALS. Amyotroph Lateral Scler 2010;11:412–13
20. Young NP, Laughlin RS, Sorenson EJ. Gadolinium enhancement of the lumbar roots in a case of ALS. Amyotroph Lateral Scler 2010;11:207–9
21. Rajabally YA, Jacob S. Chronic inflammatory demyelinating polyneuropathy–like disorder associated with amyotrophic lateral sclerosis. Muscle Nerve 2008;38:855–60
22. Kimura J. Kugelberg Lecture. Principles and pitfalls of nerve conduction studies. Electroencephalogr Clin Neurophysiol Suppl 1999;50:12–15
23. Llado J, Haenggeli C, Pardo A, et al. Degeneration of respiratory motor neurons in the SOD1 G93A transgenic rat model of ALS. Neurobiol Dis 2006;21:110–18
24. Azzouz M, Leclerc N, Gurney M, et al. Progressive motor neuron impairment in an animal model of familial amyotrophic lateral sclerosis. Muscle Nerve 1997;20:45–51
25. Kennel PF, Finiels F, Revah F, et al. Neuromuscular function impairment is not caused by motor neurone loss in FALS mice: An electromyographic study. Neuroreport 1996;7:1427–31
26. Mancuso R, Santos-Nogueira E, Osta R, et al. Electrophysiological analysis of a murine model of motoneuron disease. Clin Neurophysiol 2011;122:1660–70
27. Boerio D, Kalmar B, Greensmith L, et al. Excitability properties of mouse motor axons in the mutant SOD1(G93A) model of amyotrophic lateral sclerosis. Muscle Nerve 2010;41:774–84
28. Navarro X, Udina E. Chapter 6: Methods and protocols in peripheral nerve regeneration experimental research. Part III. Electrophysiological evaluation. Int Rev Neurobiol 2009;87:105–26
29. de Carvalho M, Swash M. The onset of amyotrophic lateral sclerosis. J Neurol Neurosurg Psychiatry 2006;77:388–89
30. Aggarwal A, Nicholson G. Detection of preclinical motor neurone loss in SOD1 mutation carriers using motor unit number estimation. J Neurol Neurosurg Psychiatry 2002;73:199–201
31. Krarup C. Lower motor neuron involvement examined by quantitative electromyography in amyotrophic lateral sclerosis. Clin Neurophysiol 2011;122:414–22
32. De Vos KJ, Grierson AJ, Ackerley S, Miller CC Role of axonal transport in neurodegenerative diseases. Ann Rev Neurosci 2008;31:151–73
33. Sotelo-Silveira JR, Lepanto P, Elizondo V, et al. Axonal mitochondrial clusters containing mutant SOD1 in transgenic models of ALS. Antioxid Redox Signal 2009;11:1535–45
34. Ligon LA, LaMonte BH, Wallace KE, et al. Mutant superoxide dismutase disrupts cytoplasmic dynein in motor neurons. Neuroreport 2005;16:533–36
35. Bilsland LG, Sahai E, Kelly G, et al. Deficits in axonal transport precede ALS symptoms in vivo. Proc Natl Acad Sci U S A 2010;107:20523–28
36. Gould TW, Buss RR, Vinsant S, et al. Complete dissociation of motor neuron death from motor dysfunction by Bax deletion in a mouse model of ALS. J Neurosci 2006;26:8774–86
37. Cappello V, Vezzoli E, Righi M, et al. Analysis of neuromuscular junctions and effects of anabolic steroid administration in the SOD1G93A mouse model of ALS. Mol Cell Neurosci 2012;51:12–21
38. Dadon-Nachum M, Melamed E, Offen D. The ''dying-back'' phenomenon of motor neurons in ALS. J Mol Neurosci 2011;43:470–77
39. Dupuis L, Loeffler JP. Neuromuscular junction destruction during amyotrophic lateral sclerosis: Insights from transgenic models. Curr Opin Pharmacol 2009;9:341–46
40. Pun S, Santos AF, Saxena S, et al. Selective vulnerability and pruning of phasic motoneuron axons in motoneuron disease alleviated by CNTF. Nat Neurosci 2006;9:408–19
41. Rocha MC, Pousinha PA, Correia AM, et al. Early changes of neuromuscular transmission in the SOD1(G93A) mice model of ALS start long before motor symptoms onset. PLoS One 2013;8:e73846
42. Schaefer AM, Sanes JR, Lichtman JW. A compensatory subpopulation of motor neurons in a mouse model of amyotrophic lateral sclerosis. J Comp Neurol 2005;490:209–19
43. Beirowski B. Concepts for regulation of axon integrity by enwrapping glia. Front Cell Neurosci 2013;7:256
44. Rouaux C, Panteleeva I, Rene F, et al. Sodium valproate exerts neuroprotective effects in vivo through CREB-binding protein–dependent mechanisms but does not improve survival in an amyotrophic lateral sclerosis mouse model. J Neurosci 2007;27:5535–45
45. Dewil M, dela Cruz VF, Van Den Bosch L, et al. Inhibition of p38 mitogen activated protein kinase activation and mutant SOD1(G93A)-induced motor neuron death. Neurobiol Dis 2007;26:332–41
46. Ravits J, Laurie P, Fan Y, et al. Implications of ALS focality: Rostral-caudal distribution of lower motor neuron loss postmortem. Neurology 2007;68:1576–82
47. Ince PG, Shaw PJ, Slade JY, et al. Familial amyotrophic lateral sclerosis with a mutation in exon 4 of the Cu/Zn superoxide dismutase gene: Pathological and immunocytochemical changes. Acta Neuropathol 1996;92:395–403
48. Devigili G, Uceyler N, Beck M, et al. Vasculitis-like neuropathy in amyotrophic lateral sclerosis unresponsive to treatment. Acta Neuropathol 2011;122:343–52
49. Hall ED, Oostveen JA, Gurney ME. Relationship of microglial and astrocytic activation to disease onset and progression in a transgenic model of familial ALS. Glia 1998;23:249–56
50. Lincecum JM, Vieira FG, Wang MZ, et al. From transcriptome analysis to therapeutic anti-CD40L treatment in the SOD1 model of amyotrophic lateral sclerosis. Nat Genet 2010;42:392–99
51. Hensley K, Floyd RA, Gordon B, et al. Temporal patterns of cytokine and apoptosis-related gene expression in spinal cords of the G93A-SOD1 mouse model of amyotrophic lateral sclerosis. J Neurochem 2002;82:365–74
52. McCombe PA, Henderson RD. The role of immune and inflammatory mechanisms in ALS. Curr Mol Med 2011;11:246–54
53. Papadimitriou D, Le Verche V, Jacquier A, et al. Inflammation in ALS and SMA: Sorting out the good from the evil. Neurobiol Dis 2010;37:493–502
54. Evans MC, Couch Y, Sibson N, et al. Inflammation and neurovascular changes in amyotrophic lateral sclerosis. Mol Cell Neurosci 2013;53:34–41
55. Graber DJ, Hickey WF, Harris BT. Progressive changes in microglia and macrophages in spinal cord and peripheral nerve in the transgenic rat model of amyotrophic lateral sclerosis. J Neuroinflamm 2010;7:8
56. Henkel JS, Beers DR, Zhao W, et al. Microglia in ALS: The good, the bad, and the resting. J Neuroimmune Pharmacol 2009;4:389–98
57. Chiu IM, Phatnani H, Kuligowski M, et al. Activation of innate and humoral immunity in the peripheral nervous system of ALS transgenic mice. Proc Natl Acad Sci U S A 2009;106:20960–65
58. Stoll G, Muller HW. Nerve injury, axonal degeneration and neural regeneration: Basic insights. Brain Pathol 1999;9:313–25
59. Kiaei M, Petri S, Kipiani K, et al. Thalidomide and lenalidomide extend survival in a transgenic mouse model of amyotrophic lateral sclerosis. J Neurosci 2006;26:2467–73.
60. Klivenyi P, Kiaei M, Gardian G, et al. Additive neuroprotective effects of creatine and cyclooxygenase 2 inhibitors in a transgenic mouse model of amyotrophic lateral sclerosis. J Neurochem 2004;88:576–82
61. Beers DR, Henkel JS, Zhao W, et al. Endogenous regulatory T lymphocytes ameliorate amyotrophic lateral sclerosis in mice and correlate with disease progression in patients with amyotrophic lateral sclerosis. Brain 2011;134:1293–314
62. Werdelin L, Boysen G, Jensen TS, et al. Immunosuppressive treatment of patients with amyotrophic lateral sclerosis. Acta Neurol Scand 1990;82:132–34
63. Gordon PH, Moore DH, Miller RG, et al. Efficacy of minocycline in patients with amyotrophic lateral sclerosis: A phase III randomised trial. Lancet Neurol 2007;6:1045–53
64. Cudkowicz ME, Shefner JM, Schoenfeld DA, e. Trial of celecoxib in amyotrophic lateral sclerosis. Ann Neurol 2006;60:22–31
65. Stommel EW, Cohen JA, Fadul CE, et al. Efficacy of thalidomide for the treatment of amyotrophic lateral sclerosis: A phase II open label clinical trial. Amyotroph Lateral Scler 2009;10:393–404
66. Napoli I, Noon LA, Ribeiro S, et al. A central role for the ERK-signaling pathway in controlling Schwann cell plasticity and peripheral nerve regeneration in vivo. Neuron 2012;73:729–42
67. Keller AF, Gravel M, Kriz J. Live imaging of amyotrophic lateral sclerosis pathogenesis: Disease onset is characterized by marked induction of GFAP in Schwann cells. Glia 2009;57:1130–42

